DEVELOPMENT AND APPLICATION OF EXPERIMENTAL AND NUMERICAL METHODS OF HYDRODYNAMICS IN THE 20th CENTURY

by

Simeon OKA, and Dubravka MELLING

Review paper
UDC: 532.5.01/.8
BIBILD: 0354-9836, 5 (2001), 1, 5-31

The development of fluid mechanics is briefly reviewed and the importance of fluid flows to heat and mass transport in nature as well as in science and engineering is outlined. The early theoretical developments are explained and it is indicated that the basic equations were available at the end of the 18th century. Methods to solve these equations for engineering flows were not, however, developed until the second half of the 20th century. This was an important period for fluid flow research during which all the experimental fluid mechanics methods, particularly the optical methods, available today were also developed. The same is true for all the numerical methods that are used very successfully nowadays to solve scientific and engineering fluid flow problems. Prof. Durst and his research groups, first at the University of Karslruhe and later at the University of Erlangen-Nürnberg, have contributed extensively to these developments. The present issue of the Journal of Thermal Science embraces publications of the heads of the research sections of his institute in Erlangen, Germany which document these contributions and is dedicated to the 60th birthday of Prof. Durst.

INTRODUCTION

Fluid flows are present everywhere in nature and are widely experienced by those people who observe nature with open eyes. They see that many processes in our natural environment are vitally dependent on the convective transport of heat and mass. Hence, without fluid motion, life in the form we know it on earth could not exist.

Figure 1 provides a chronological summary of important scientists in fluid mechanics. It gives an impression when certain contributions to the development of the theory of fluid mechanics were made, but experimental or numerical techniques are not

introduced in this chart. Measuring techniques will be reviewed in the paper emphasising those techniques to which Prof. Durst and his co-workers were able to make world wide recognised contributions. The contributions of Prof. Durst's research groups also cover numerical techniques and their application to fluid flow.

Figure 1. Historical record of scientists contributing to the development of fluid mechanics

The technical importance of fluid flows is also easily observable in many engineering fields where heat and mass transfer processes are strongly controlled by fluid motions. The rate of conversion of chemically bonded energy into heat by non-premixed combustion is mainly controlled by the flow transport of the chemically reacting species and heat engines, for example, could not fulfil their function without the corresponding flow. Hence, fluid flows are essential in many fields where engineering equipment is used.

This publication summarises the development of fluid flow investigations that can be carried out using modern experimental and numerical techniques as they were developed in the last fifty years. It is pointed out that these techniques can be used successfully for the solution of flow problems in science and engineering. An outlook is given on the golden age of fluid mechanics that lies ahead of us, as Prof. Durst has pointed out in recent summaries of fluid mechanics developments covering the last fifty years. The present paper is based on the material he has used for several invited lectures in the years 1999 to 2001.

Prof. Durst's contributions to fluid flows have always started out with fundamental investigations yielding knowledge which was used for developments of practical relevance. These developments brought new ideas into engineering fluid mechanics and have frequently resulted in commercial products and the foundation of new companies.

The above introductory remarks that stress the importance of fluid flows might explain why fluid mechanics has a history that goes back as long as records of human culture exist. Although there were contributions by Archimedes and Sixtus Julius Francius as well as first flow visualisations by Leonardo da Vinci, fluid mechanics as a science only began under G. Galilei in the 17th Century. This is indicated in figure 1 which shows the long list of researchers who have made contributions to the subject over the last four centuries. Among the fluid mechanics scientists of the 17th to the 19th century one finds the names of famous mathematicians and physicists indicating that fluid mechanics as a basic engineering subject is fairly new in a historical context. Nowadays, any serious engineering education in fields such as aeronautical engineering, mechanical engineering and chemical engineering is heavily based on a sound fluid mechanics education. This will also continue in the future.

Major contributions were made by Newton, Euler, Lagrange, Navier and Stokes to the derivation of the basic equations of fluid mechanics. From the dates in Fig. 1 one can see that by the end of the 18th century the equations of fluid mechanics were basically known in the general form given below for ρ = constant:

Continuity equation:

$$\frac{\partial \rho}{\partial t} + \frac{\partial (\rho U_i)}{\partial x_i} = 0 \tag{1}$$

Momentum equation (j =1, 2, 3):

$$\rho\left(\frac{\partial U_j}{\partial t} + U_i \frac{\partial U_j}{\partial x_i}\right) = -\frac{\partial P}{\partial x_j} - \frac{\partial \tau_{ij}}{\partial x_i} + \rho g_j \tag{2}$$

$$\tau_{ij} = -\mu\left(\frac{\partial U_j}{\partial x_i} + \frac{\partial U_i}{\partial x_j}\right) + \frac{2}{3}\delta_{ij}\mu\frac{\partial U_k}{\partial x_k}$$

For ρ = constant, the three velocity components and the pressure can be named as the unknowns of the above set of four differential equations. Hence four unknowns and four partial differential equations exist and, so all fluid flow problems seem to be soluble if the appropriate initial and boundary conditions exist.

Although these equations were known by the end of the 18th century, methods for their solution did not exist. The present paper stresses that all methods to solve the above set of equations for engineering flow problems were developed in the second half of the 20th century following tremendous advances in numerical methods and computer power. As Fig. 2 shows, high-performance computer developments have provided an increase in computational speed by a factor 10 every 5 years. In the last three decades, a factor of 10 every 8 years was also achieved by advanced numerical techniques. All these developments together now permit numerical solutions of the above set of equations for engineering problems.

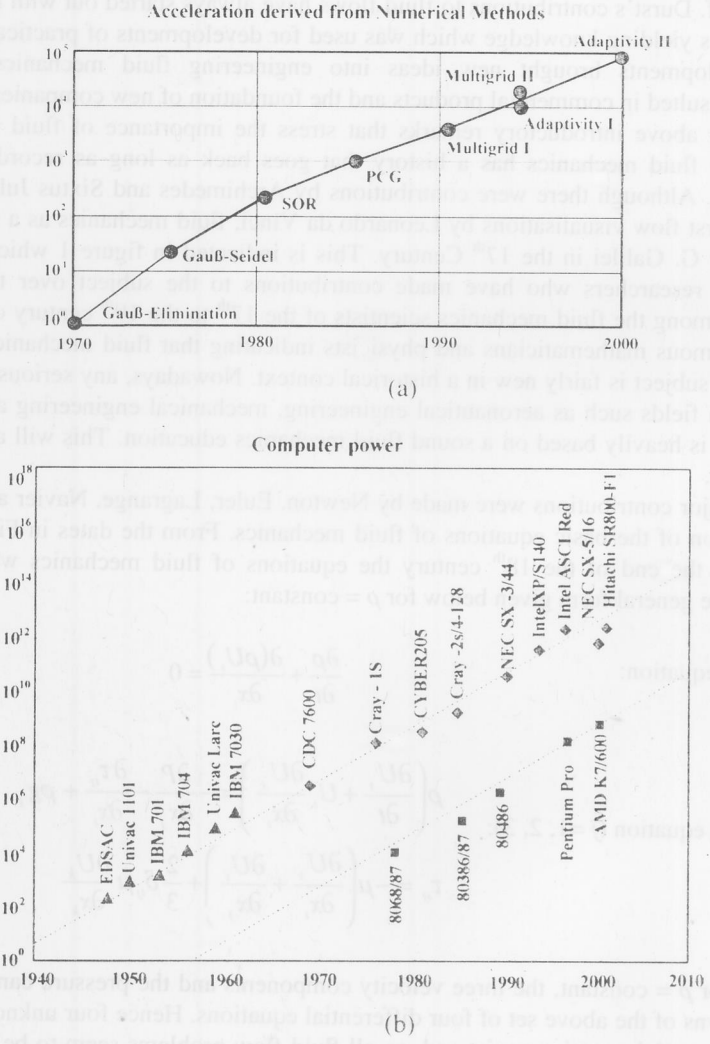

Figure 2. Speed-up of numerical computations due to numerical methods (a) and increase in computer power (b)

The developments in numerical solutions to the above set of equations of fluid mechanics in the second half of the 20th century were accompanied by tremendous developments in the field of experimental fluid mechanics. The development of fast electronic components, lasers, integrated optics, sensors, micro-techniques, *etc.*, has resulted in a wide range of measuring techniques for studying fluid flows. The present paper concentrates on the development of optical techniques such as photography and

cinematography, laser-Doppler anemometry, phase-Doppler anemometry, particle image velocimetry and other field methods. The developments are summarised and emphasis is given to those developments carried out in Professor Durst's research group initially at the University of Karlsruhe and later at the University of Erlangen-Nürnberg.

FLOW VISUALIZATION: PHOTOGRAPHY AND CINEMATOGRAPHY

It is difficult to define clearly where and when fluid mechanics as a science started. However, the first contribution that had an impact on the subject as it is treated today is the flow visualisation carried out by Leonardo da Vinci (1452-1519). Since this early work, flow visualisation has advanced with major developments being based on modern illumination techniques, as well as developments in photography and cinematography. This is indicated in Fig. 3, which compares photographic records of flows with the early sketches of observed vortex motions by Leonardo da Vinci.

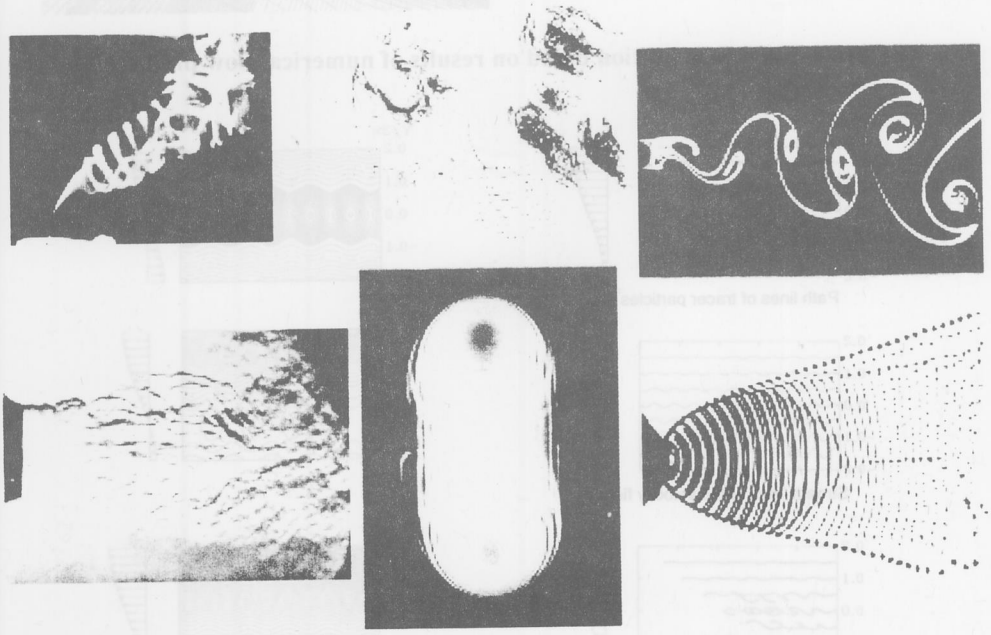

Figure 3. Flow visualisation is the start of good fluid mechanics research

A summary of flow visualisation results is given in the Album of Fluid Motion assembled by van Dyke [1]. This assembly of pictures makes clear that photographic records of fluid motion can result in path lines, streak lines or streamlines of the flow. All of them are difficult to analyse in terms of local velocity information or to obtain results in the terminology of the basic equations of fluid mechanics. Nevertheless, they provide a good physical insight into the flow so that it has become common practice also to visualize the results of flow predictions, *e. g.* see Fig. 4.

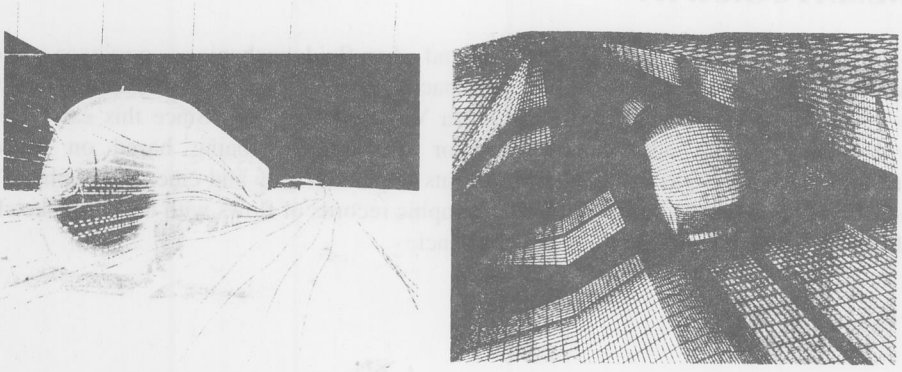

Figure 4. Flow visualisation based on results of numerical flow predictions

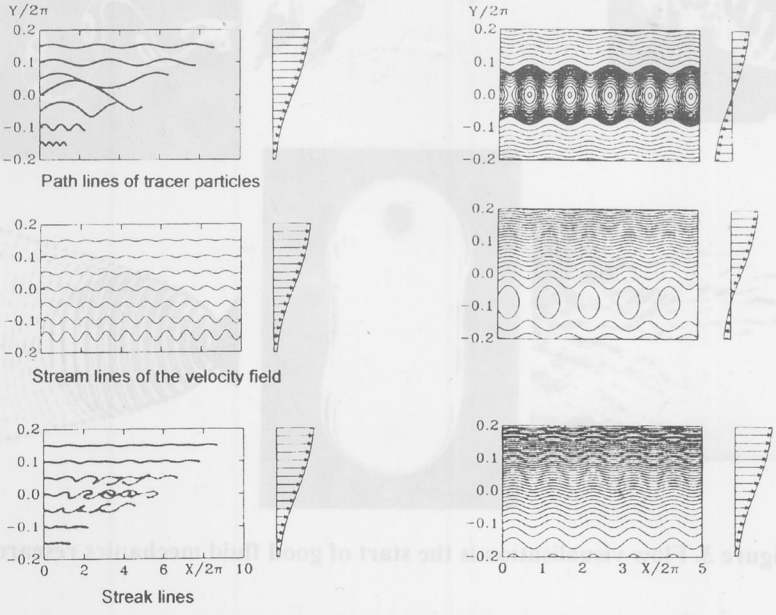

Figure 5. Demonstration of complex flow information in path, streak and stream lines

The impressive pictures that flow visualisation provide often lead the flow researcher to forget that it is very difficult to interpret correctly the resultant flow motions. This was outlined by Hama [2] and demonstrated by Eckelmann [3], from which the example in Fig. 5 is taken.

Although Leonardo da Vinci showed the power of flow visualisation as a basis for physical insight into flows, and modern methods of flow illumination and recording of fluid motion have become available, flow visualisation is not applied to its best in modern fluid mechanics. The turbulent flows that are being studied these days yield complex flow visualisation pictures and quantitative information is difficult to obtain by flow visualisation.

LASER-DOPPLER ANEMOMETRY

During the second half of the 20th century, rapid developments in electronics and optics components provided the basis for the advancement of methods to measure local and time resolved flow velocities. Fast operating electronic feedback amplifiers permitted the development of constant temperature hot wire anemometry, *e. g.* see Bruun [4]. With the help of this technique, first detailed velocity information became available about turbulent flows, providing an insight into the complexity of turbulence. Detailed turbulent flow studies provided the basis for advanced analytical treatments of flows, *e. g.* see Lumley [5]. However, the application of hot wire anemometry was, and still is, limited to flows with low levels of turbulence. The method also is intrusive, yielding flow disturbances that are unacceptable in recirculating flows. These shortcomings of hot-wire anemometry triggered new developments. Laser-Doppler anemometry emerged from these development efforts, providing new means to study fluid flows.

Light scattered by tracing particles

Large particles scatter light well but do not follow fast variations of velocity fluctuations of the fluid.

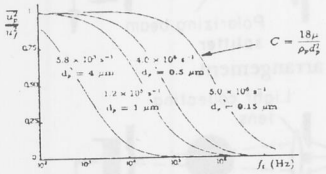

$$m_p \frac{du_p}{dt} = c_D A \frac{\rho_f}{2}\left(u_p - u_f\right)^2$$

$$\frac{\overline{u_p^2}}{\overline{u_f^2}} = \int_0^\infty \frac{\Omega^{(1)}}{\Omega^{(2)}} E(\omega)\, d\omega$$

Particles employed in laser-Doppler anemometry must not only be good scatters but also follow the flow very well. They must also be chemically and physically stable, non-poisonous, cheap, easy to get, etc.

Figure 6. Scattering particles with high scattering efficiency and good flow velocity response

Laser-Doppler anemometry is a well documented measuring technique, *e. g.* see Durst, Melling and Whitelaw [6]. Light scattering particles are needed that follow the flowing fluid so that the particle velocity is close to that of fluid, *e. g.* see van de Hulst [7], Kerker [8] and Hjelmfelt and Mockros [9]. These basic requirements for LDA scattering particles are summarised in Fig. 6.

From the many scattering mechanisms that can be used to deduce the local particle velocity from laser frequency shift information, *e. g.* see Durst [10], the dual scattering beam laser-Doppler effect was shown to be the most efficient and most robust for use in LDA velocity measurements. Hence optical systems of the type shown in Fig. 7 are these days employed to measure local flow velocities by laser-Doppler anemometry. Multi-component anemometers, as indicated in Fig. 8, are available.

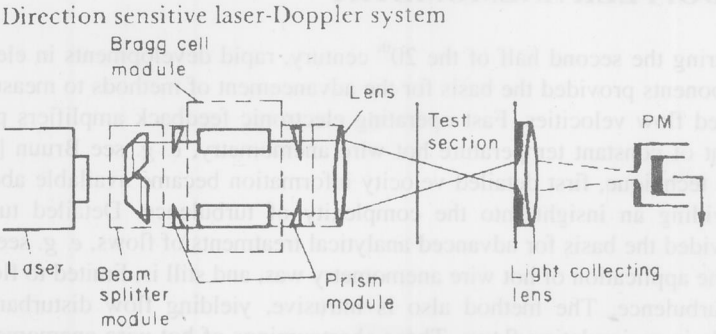

Figure 7. Dual beam laser-Doppler optical system

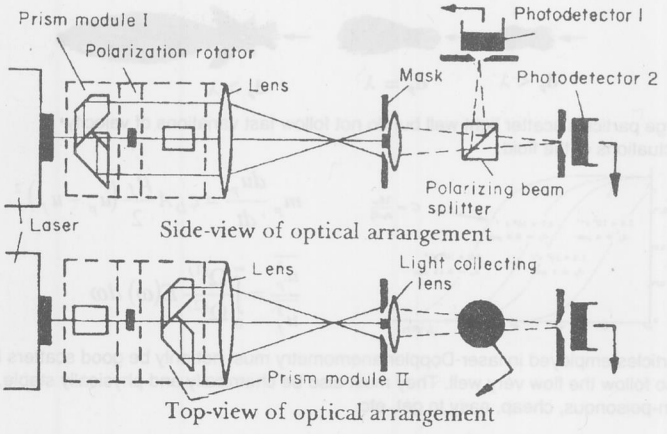

Figure 8. Two-component laser-Doppler optical system

Laser-Doppler anemometers can be applied to carry out flow measurements that are not feasible with any other fluid flow measuring technique. Figure 9 shows a test facility providing a fully developed channel flow. With the help of a laser-Doppler anemometer, detailed flow measurements were carried out, yielding the velocity information sketched in Fig. 9. Analysing these data revealed a Reynolds number dependence of the wall value of the turbulence intensity, as shown in Fig. 10.

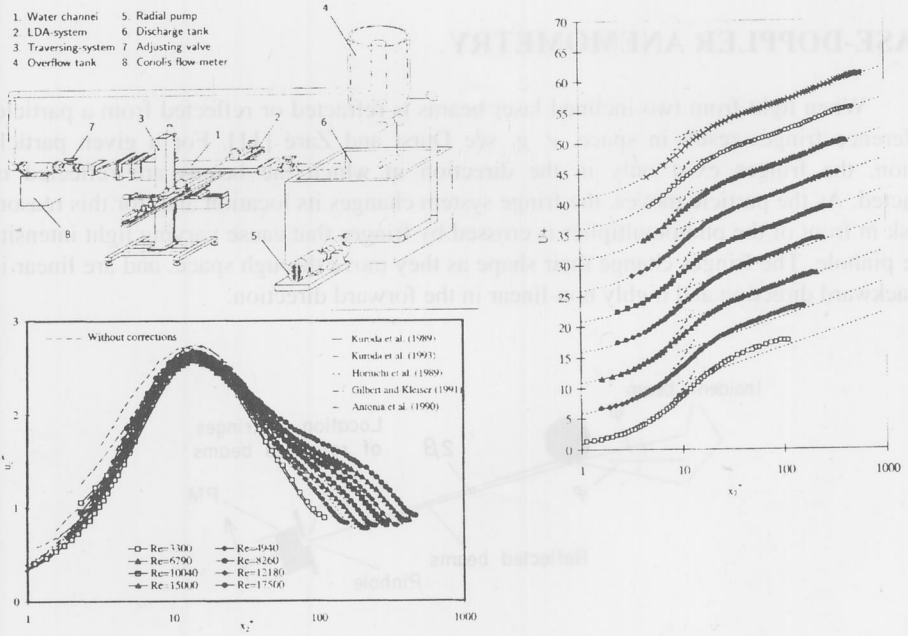

Figure 9. LDA investigations of turbulent channel flows

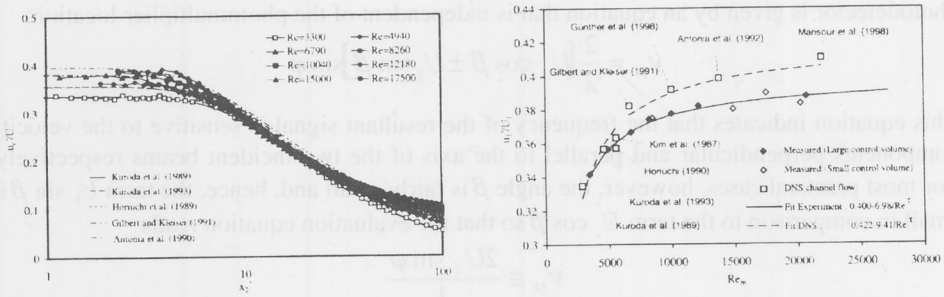

Figure 10. Wall values of tubulence levels in fully developed channel flows

It is interesting to note that at present the Reynolds number dependence of the wall value of the turbulence intensity is not understood. Both experimental and numerical studies show this dependence, but there are differences between the experimental and numerical results which cannot readily be explained. They may be due to the finite sizes of the computational grids and the measuring control volume of the LDA systems. The evaluation of the final data requires finite size volume corrections; the experimental data in Fig. 10 were obtained with optical systems with measuring control volumes of different sizes.

PHASE-DOPPLER ANEMOMETRY

When light from two inclined laser beams is refracted or reflected from a particle, interference fringes result in space, *e. g.* see Durst and Zaré [11]. For a given particle location, the fringes exist only in the direction in which the beams are reflected or diffracted. As the particle moves, the fringe system changes its location and, for this reason, a mask in front of the photomultiplier is crossed by fringes that cause varying light intensity at the pinhole. The fringes change their shape as they move through space, and are linear in the backward direction and highly non-linear in the forward direction.

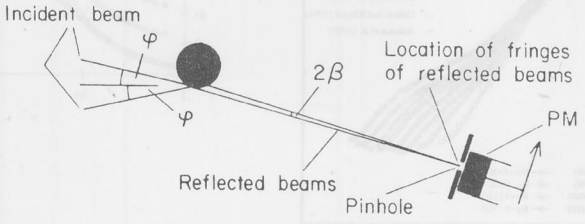

Figure 11. Phase-Doppler measurements in two-phase flows

Irrespective of the shape of the fringes, the derivation by Durst and Zaré [11] revealed that the resultant frequency due to the fringes crossing a mask in front of the photodetector is given by an equation that is independent of the photomultiplier location:

$$\nu_D = \frac{2}{\lambda}\left[U_\perp \cos\beta \pm U_\parallel \sin\beta\right]\sin\varphi$$

This equation indicates that the frequency of the resultant signal is sensitive to the velocity components perpendicular and parallel to the axis of the two incident beams respectively. For most practical cases, however, the angle β is fairly small and, hence, the term $U_\parallel \sin\beta$ is small in comparison to the term $U_\perp \cos\beta$ so that the evaluation equation reads

$$\nu_D \cong \frac{2U_\perp \sin\varphi}{\lambda}$$

The angle β is a function of the angle between the two incident beams and the ratio of detector distance to particle diameter. For large values of L/R, where L is the detector distance and R is the particle radius, the angle β tends to zero; β also decreases with decreasing angle φ. The same arguments apply to light beams refracted by transparent particles. In this case, linear interference fringes result in the forward direction and the Doppler frequency is not dependent on the velocity component parallel to the axis of the two incident light beams. The equation for the Doppler frequency reads in this case

$$\nu_D \cong \frac{2U_\perp(\sin\varphi - \sin\beta)}{\lambda} \tag{3}$$

In addition to measuring the particle velocity, phase Doppler systems also permit the measurement of particle size by measuring the phase difference between signals from two detectors, as indicated in Fig. 12. The resultant equation used to deduce the particle diameter from the measured phase difference depends on the location of the photodetector with respect to the transmission optics, *i. e.* whether reflected or refracted light is used for signal detection. Hence information of the kind shown in Fig. 13 is obtainable with phase-Doppler systems at every location in a flow field. Therefore, particulate two-phase flows can be studied by phase-Doppler anemometry.

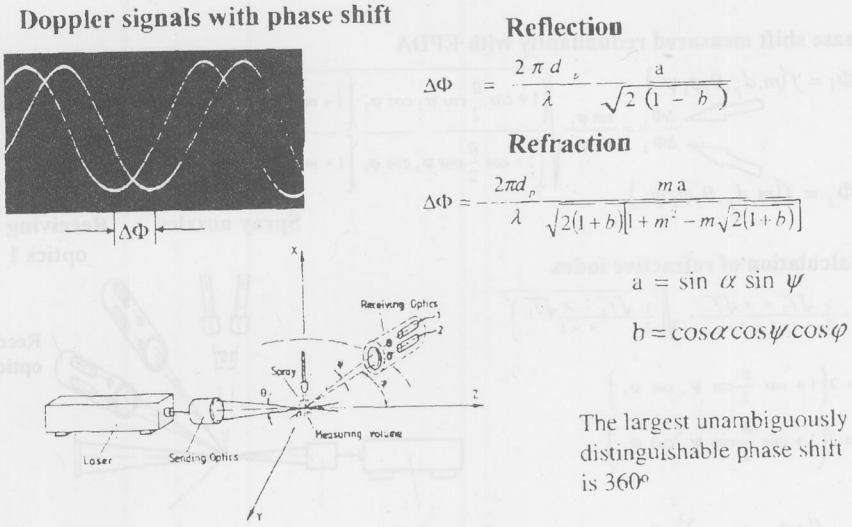

Figure 12. Principle of operation and sketch of optics of a phase-Doppler anemometer

Spray measurement results

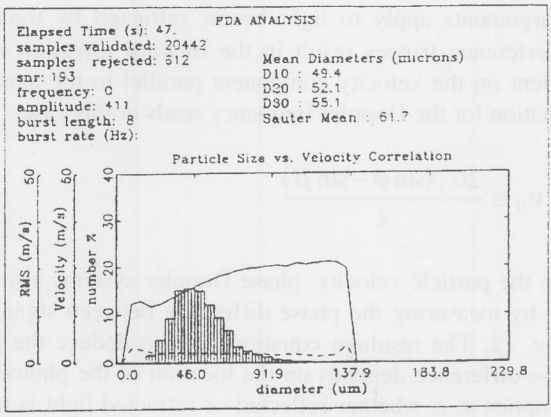

Information achieved:

- **Drop size number distribution**
- **Size / velocity correlation**
- **Mean / RMS velocity correlation**
- **Moments of the drop size spectrum**

Figure 13. Typical result of local time and velocity measurements in sprays

Phase shift measured redundantly with EPDA

$$\Delta\Phi_1 = f(m, d_p, \theta, \varphi_1, \psi_1)$$

$$\Delta\Phi_2 = f(m, d_p, \theta, \varphi_2, \psi_2)$$

$$\frac{\Delta\Phi_1}{\Delta\Phi_2} = \frac{\sin\psi_1}{\sin\psi_2}\sqrt{\frac{\left(1+\cos\frac{\theta}{2}\cos\psi_2\cos\varphi_2\right)\left[1+m^2-m\sqrt{2\left(1+\cos\frac{\theta}{2}\cos\psi_2\cos\varphi_2\right)}\right]}{\left(1+\cos\frac{\theta}{2}\cos\psi_1\cos\varphi_1\right)\left[1+m^2-m\sqrt{2\left(1+\cos\frac{\theta}{2}\cos\psi_1\cos\varphi_1\right)}\right]}}$$

Calculation of refractive index

$$m = -\frac{1}{2}\frac{\sqrt{f_2}-A\sqrt{f_1}}{A-1} + \sqrt{\left(\frac{1}{2}\frac{\sqrt{f_2}-A\sqrt{f_1}}{A-1}\right)^2 - \frac{1}{A-1}}$$

$$f_1 = 2\left(1+\cos\frac{\theta}{2}\cos\psi_1\cos\varphi_1\right)$$

$$f_2 = 2\left(1+\cos\frac{\theta}{2}\cos\psi_2\cos\varphi_2\right)$$

$$A = \left(\frac{\Delta\Phi_1\sin\psi_2}{\Delta\Phi_2\sin\psi_1}\right)^2\frac{f_1}{f_2}$$

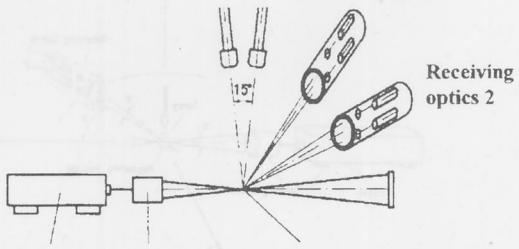

Figure 14. Optical system for extended phase-Doppler measurements

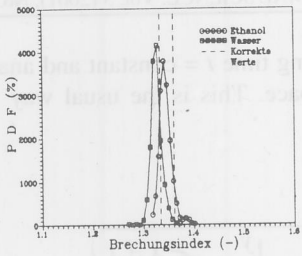

Refractive index distributions measured in monodisperse drop streams.
Water and ethanol can be distinguished.

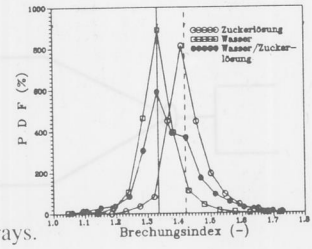

Water $m_w = 1.334$
Ethanol $m_e = 1.361$
Sugar water 50/50 $m_z = 1.421$
Refractive indices in mixed polydisperse sprays.

Figure 15. Refractive index measurements using extended phase-Doppler anemometer

The phase-Doppler method has also been extended to yield information on the refractive index of the light refracting particles in a flow. Extended phase-Doppler anemometers have been suggested for this purpose using four detectors located in different directions. This is indicated in Fig. 14, which also provides the equation used for particle refractive index measurements utilising the ratio of two phase difference measurements. Results of application of an extended phase-Doppler system are shown in Fig. 15.

Without any doubt, phase-Doppler anemometers work best with spherical particles. The application of PDA systems could lead to interesting results on laminar and turbulent particulate two-phase flows. Fluid mechanics research should concentrate on using the phase-Doppler anemometers that are available rather than placing emphasis on the extension of existing phase-Doppler anemometers to yield information on particle material, measurements of non-spherical particles, *etc.*

There have been numerous contributions to the development of phase-Doppler anemometry and a good summary of the earlier work was given by Hirleman [12], with useful later contributions by Naqwi *et al.* [13] and Gouesbet *et al.* [14].

PARTICLE IMAGE VELOCIMETRY AND OTHER FIELDS

When flows are described in terms of the local time varying velocity field, *i. e.* as $U_j(x_i, t)$, there are basically two ways to analyse experimental and/or numerical data.

- *Local analysis:* This approach fixes the measuring location x_i = constant and analyses the velocity data as a time series. This is the usual way in which hot wire and laser Doppler anemometers are operated.

- *Spatial analysis:* This approach fixes the measuring time t = constant and analyses the velocity data as a distribution of velocities in space. This is the usual way in which particle image velocimetry works.

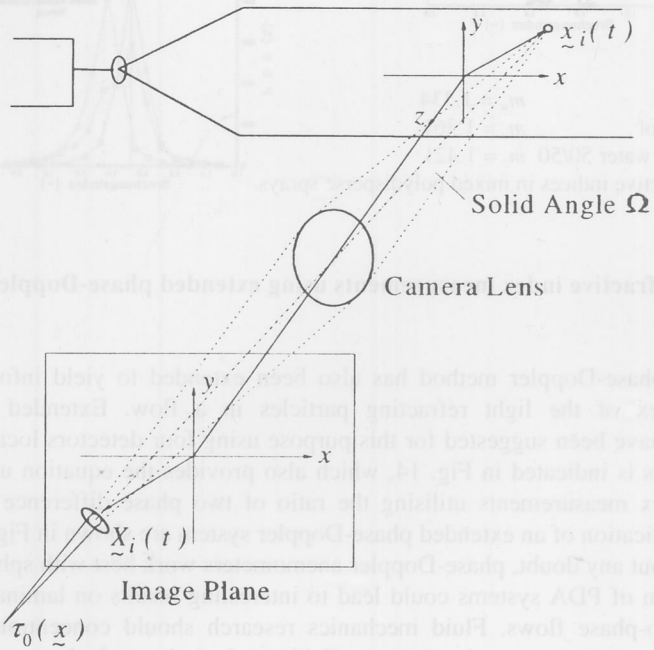

Figure 16. Pulsed illuminating beam and photographic image plane

Particle image velocity (PIV) uses an optical set-up of the kind shown in Fig. 16, as described by Adrian [16]. Field information results are sketched in Fig. 17. In the illuminated plane of thickness Δs, all those pairs of components of the velocity fields are recorded that were represented by a scattering particle and fulfilled the following requirements:

- the particle was large enough to scatter sufficient light to yield a good record of the particle,
- the particle was small enough, considering its size, density and shape, to follow the flow,
- the velocity component of the particle perpendicular to the light sheet was small so that the following relationship holds:

$$U_{\perp} \leq \frac{\Delta s}{\Delta t}$$

where $U_{\perp}$ = velocity component perpendicular to light sheet, Δs = thickness of illuminated sheet and Δt = time between particle images. Hence conditional information on the velocity field is obtained.

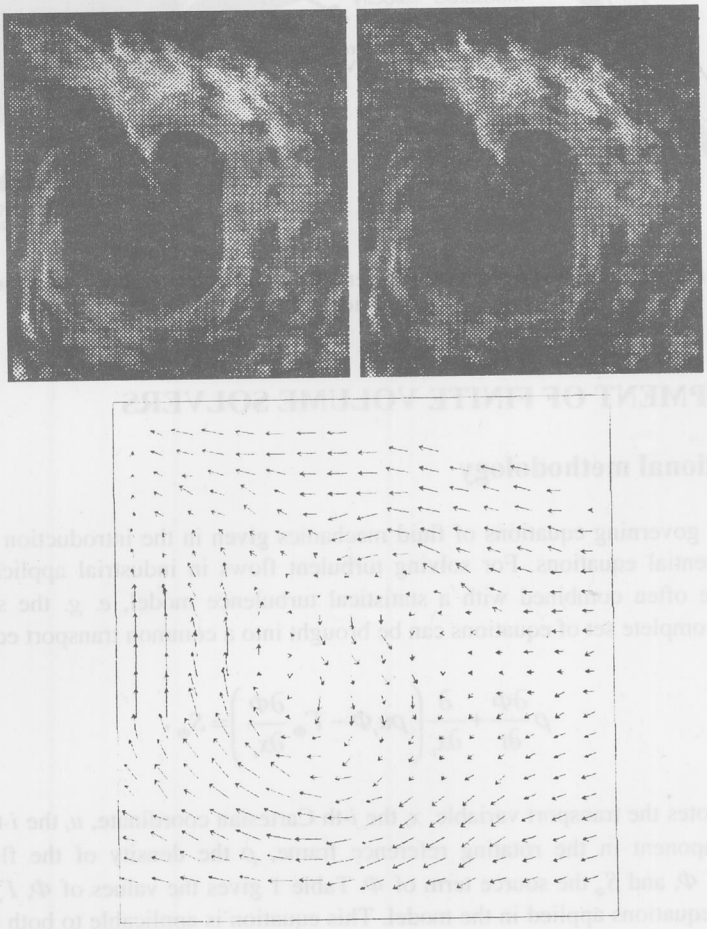

Figure 17. Flow against a vertical plate visualised by smoke and velocity distribution measured by PIV, results by Uemura *et al.* [15]

Another method that should be mentioned as a field method is Doppler global velocimetry (DGV), *e. g.* see Meyers and Lee [17]. With this technique the absorption properties of iodine are used to obtain direct Doppler shift information for the scattered light optical systems of the kind shown in Fig. 18.

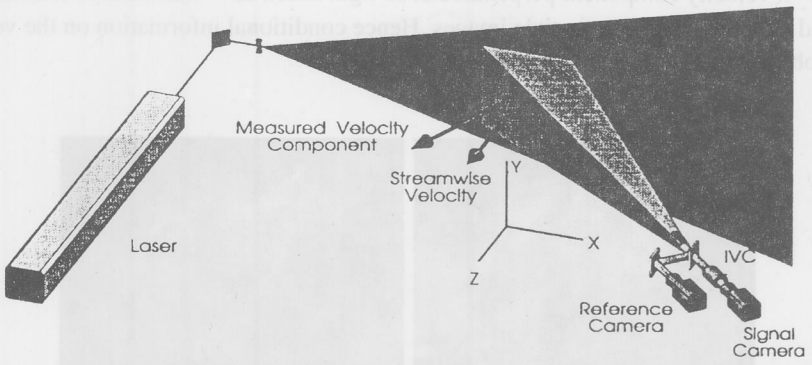

Figure 18. Sketch of optical arrangement of Doppler global velocimeter, Meyers and Lee [17]

DEVELOPMENT OF FINITE VOLUME SOLVERS

Computational methodology

The governing equations of fluid mechanics given in the introduction are a set of partial differential equations. For solving turbulent flows in industrial applications these equations are often combined with a statistical turbulence model, *e. g.* the standard k-ε model. The complete set of equations can be brought into a common transport equation:

$$\rho\frac{\partial\Phi}{\partial t}+\frac{\partial}{\partial x_i}\left(\rho u_i\Phi-\Gamma_\Phi\frac{\partial\Phi}{\partial x_i}\right)=S_\Phi, \tag{4}$$

where Φ denotes the transport variable, x_i the i-th Cartesian coordinate, u_i the i-th Cartesian velocity component in the rotating reference frame, ρ the density of the fluid, Γ_Φ the diffusivity of Φ, and S_Φ the source term of Φ. Table 1 gives the values of Φ, Γ_Φ and S_Φ for all transport equations applied in the model. This equation is applicable to both a stationary and a rotating frame of reference. The velocity vector in a stationary reference frame $\underline{U}$ and the velocity vector in a rotating reference frame $\underline{u}$ are related by $\underline{U}=\underline{u}+\underline{\omega}\times\underline{x}$ where $\underline{\omega}=(\omega_1, \omega_2, \omega_3)$ represents the angular velocity vector and $\underline{x}=(\omega_1, \omega_2, \omega_3)$ the position relative to the rotation axis.

The numerical solution method is based on a fully conservative finite volume discretization on non-orthogonal boundary fitted grids with a non-staggered arrangement of the variables. Second order discretization is used for all terms (central differences, linear interpolation) together with flux blending and a deferred correction approach for the convective fluxes.

Table 1. Transport variable Φ, diffusivity Γ_Φ and source term S_Φ for all transport equations applied in the model. Additional relations and constants not mentioned in the text: $\mu_t = c_\mu \rho(k^2/\varepsilon)$, $c_\mu = 0.09$, $\sigma_k = 1.0$, $\sigma_\varepsilon = 1.3$, $c_{\varepsilon 1} = 1.44$, $c_{\varepsilon 2} = 1.92$

Conservation variable	Φ	Γ_Φ	S_Φ
Mass	1	0	0
Momentum (j-th component)	u_j	$\mu+\mu_t$	$-\frac{\partial p}{\partial x_j}+\frac{\partial}{\partial x_i}\left((\mu+\mu_t)\frac{\partial u_j}{\partial x_i}\right)$ $+2\varepsilon_{mnj}u_m\omega_n-\varepsilon_{mnj}\omega_m\left(\varepsilon_{pqn}\omega_p x_q\right)$
Turbulent kinetic energy	k	$\mu+\frac{\mu_t}{\sigma_k}$	$\mu_t\left(\frac{\partial u_i}{\partial x_k}+\frac{\partial u_k}{\partial x_i}\right)\frac{\partial u_i}{\partial x_k}-\rho\varepsilon$
Dissipation rate of k	ε	$\mu+\frac{\mu_t}{\sigma_\varepsilon}$	$\frac{\varepsilon}{k}c_{\varepsilon 1}\mu_t\left(\frac{\partial u_i}{\partial x_k}+\frac{\partial u_k}{\partial x_i}\right)\frac{\partial u_i}{\partial x_k}-c_{\varepsilon 2}\rho\frac{\varepsilon^2}{k}$

Based on the continuity equation, a pressure correction equation is derived according to the SIMPLE algorithm. The linearized equations for the velocity components, the pressure correction and other scalar variables are assembled and solved sequentially, where the ILU approach of Stone is employed as a linear system solver. Outer iterations are performed to take into account the non-linearities, the coupling of the variables, and the effects of grid non-orthogonality, which are treated explicitly in all equations. In the case of unsteady computations, the discretization of the time derivatives is done by a three time level, second order fully implicit scheme.

Block structured grids, where the blocks are globally unstructured but the grids are locally structured, are used as they can be viewed as a compromise between the high geometric flexibility of fully unstructured grids and the high numerical efficiency achieved on globally structured grids. The coupling of the blocks along the block interfaces, *i. e.* the transfer of information among neighboring blocks, is realized by adding auxiliary control volumes along the block interfaces containing the corresponding boundary values of the neighboring block. To ensure the coupling of the subdomains, the boundary data in the auxiliary control volumes of neighboring blocks is updated after each inner iteration of the iterative linear system solver. More details can be found in [18, 19].

The numerical simulation of practically relevant flows often involves the handling of complex geometries and complex physical and chemical phenomena, requiring the use of very fine grids and small time steps in order to achieve the necessary numerical accuracy. In recent years, intensive research has been undertaken to improve the performance of flow computations in order to extend their applicability to a cost effective solution of practically relevant flow problems. These improvements concerned both acceleration by the use of more efficient solution algorithms such as multi-grid methods and acceleration by the use of more efficient computer hardware such as high performance parallel and vector parallel

computers (see paper by Breuer *et al.* in this issue). Care has to be taken in order to benefit from both the efficient numerical techniques and parallel computing. In the present method, high numerical efficiency is obtained by a global nonlinear multi-grid method with a pressure correction smoother also ensuring only slight deterioration of the convergence rate with increasing processor numbers. The results presented here illustrate that the high performance of the underlying sequential multi-grid algorithm can be largely retained in the parallel implementation.

The three dimensional flow around a circular cylinder in a square channel at Re = 20 was considered; this represents one of the test cases for benchmark computations gathered at LSTM-Erlangen. The problem was computed with the multi-grid method with nested iteration for different grid sizes, where the coarsest grid with 768 CVs and up to five grid levels were used. With increasing number of fine grid CVs, the number of processors was also increased (not linearly). In Table 2, the computing times and numbers of fine grid iterations are given for the computations, and for comparison the corresponding values for the single grid computation are also indicated.

Table 2. Computing times and numbers of fine grid iterations (in parentheses) for single grid (SG) and full multi-grid (MG + NI) methods with corresponding acceleration factors (with respect to computing time) for different numbers of processors and control volumes for the flow around a circular cylinder

Method	6144 CV P = 1	49152 CV P = 8	393216 CV P = 32	3145728 CV P = 128
SG	1679 (58)	6041 (207)	40604 (675)	–
MG + NI	624 (25)	783 (27)	1738 (26)	2630 (25)
Acceleration factor	2.7	7.7	23.4	> 70

Several conclusions can be drawn from the results. The multi-grid method is significantly superior to the corresponding single grid computation. Whereas the single grid method shows a typical linear increase in iteration numbers with grid refinement, the iteration numbers for the multi-grid method change only slightly. When the number of processors is increased with an increasing number of control volumes, the multi-grid method gives a very good scale-up in the computing time. Because of the increase in iteration numbers caused by the decoupling due to the grid partitioning this is not the case for the single grid computations. If one compares, for instance, the results for P = 8 and P = 32, which correspond to grid sizes per processor differing by a factor of two, one can see that a good parallel efficiency is obtained. We have scale-ups of 97% for SG and 90% for MG + NI. The lower value when using MG is due to the increase in work on coarser grids, where the portion of communication relative to the arithmetic operations is larger.

Examples for the solution of engineering problems

The CFD techniques developed at LSTM Erlangen have been used for the solution of a large variety of practical applications, *e. g.*:

- side wind effects on high speed trains, [20, 21]
- turbulent flow in stirred vessels, [22 - 24]
- fluid-structure interaction for civil engineering applications, [25, 26]
- flow and heat transfer in the melt of a Czochralski crucible, [27 - 30]
- turbulent flow around bluff bodies, [31 - 36]
- heat transfer of hot wires in near wall configuration, [37, 38]

These examples include internal and external laminar as well as turbulent flows. For the turbulent case all three relevant techniques are applied, namely Reynolds averaged Navier-Stokes equations (RANS), direct numerical simulation (DNS), and last but not least large eddy simulation (LES). In the present paper one example for a laminar flow and one example for turbulent case including heat transfer are considered in detail.

Flow and heat transfer of hot wire in near wall configuration

Hot wire near wall correction plays an important role in flow measurement. Since several decades, it is not clear in the literature whether no correction, a small positive correction or a negative correction is needed in the case of walls consisting of poorly conducting materials. The physical mechanism concerned also remains not fully understood.

At LSTM Erlangen, a detailed numerical investigation of the two dimensional laminar flow and heat transfer around a single circular cylinder located close to walls of different materials was performed to study the hot wire near wall correction. The conjugated heat conduction in the solid wall was taken into account to bridge the discrepancy between the previous theoretical models and the practical situation. Simulations were carried out for several realistic wall materials (aluminium, with thermal conductivity ratio to air $k^*=k_w/k_{air}=9186$; glass, $k^*=29.6$; plexiglas, $k^*=7.2$) and some theoretical materials with $k^*=1$, 0.1, and 0.01, respectively. The computed results show good agreement with experimental data in the literature. Accurate correction curves for hot wire anemometers were obtained with respect to different wall materials. Based on the present study, the physical mechanism of the wall effect has been revealed and the existing confusions can be clarified.

The predicted velocity corrections expressed by the correction factor $C_U=U_0/U_{appa}$ are presented in Fig. 19 for walls consisting of mirror glass and plexiglas (poorly conducting materials). Here U_0 is the actual and U_{appa} the apparent velocity value, respectively. As demonstrated, the velocity correction curves can be divided into three regions: (a), no correction ($C_U = 1$); (b), negative ($C_U > 1$) and (c), positive ($C_U < 1$) corrections with respect to different wire to wall distances. This phenomenon could also be clearly recognized in some experimental data (see Fig. 19) in the literature but was ignored up to now.

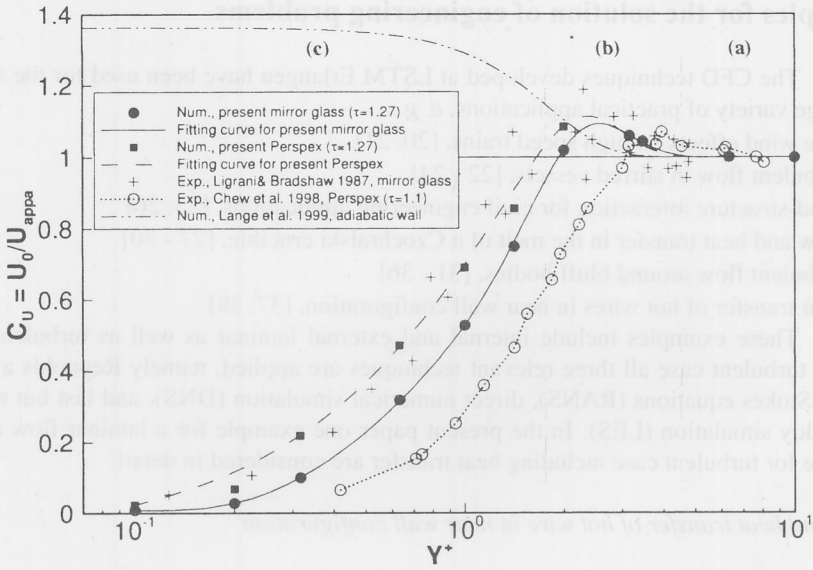

Figure 19. Comparison of numerical and experimental values of the velocity correction factor C_U in cases of walls with low conductivities

(a) $C_U = 1.0$ (b) $C_U > 1.0$ (c) $C_U < 1.0$

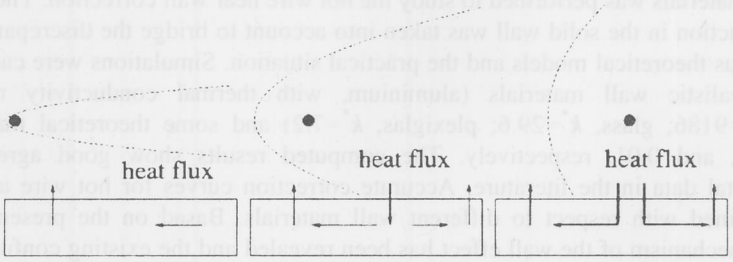

Figure 20. Schematic temperature influence region of a hot-wire and the heat exchange process between the fluid and the solid wall at various wire to wall distances Y^+

By means of dimensional analysis and according to the temperature isolines both in the flow region and in the solid wall, the physical mechanism (sketched in Fig. 20) for the distinct correction behaviour can be understood. Neglecting the shear effect, a parabolic expression for the temperature influence region of a wire in the near wall measurement is obtained:

$$\frac{X}{D} = \mathrm{Pr}\left(\frac{Y}{D}\right)(Y^+)^2 - \frac{1}{4\,\mathrm{Pr}\,\mathrm{Re}_D} \qquad (5)$$

When a hot wire comes close to a wall below a certain value of Y^+, heat transfer from the fluid into the wall material occurs at the interface between the temperature influencing region of a hot wire and the solid wall. The heat flux from the fluid is then conducted both in the upstream and downstream directions in the solid wall and fed back into the flow when the fluid temperature is lower than that in the solid wall. In case (a), this „temperature influencing region-wall" interaction occurs far away downstream from the wire location and the heat „feed-up" through the wall conduction has no evident effect on the hot wire heat loss due to large values of Y^+. As a result, no correction is required ($C_U \approx 1.0$). In case (b), the interaction between the temperature influencing region and the wall occurs at a smaller distance downstream of the wire. the feed-back heat flux from the upstream conduction in the wall warms up the oncoming fluid which will flow over the wire. As a result, heat loss from the wire is reduced, *i. e.* $C_U > 1$. In case (c), the parabolic influencing region collides with the wall in the proximity of the wire location. The heat loss from the wire is significantly enhanced due to the much higher conductivity of the wall material compared with the fluid. The enhancing effect becomes dominant over the restraining effect arising from the heat „feed-up". Thus, positive corrections are observed ($C_U < 1$). In conclusion, based on this detailed numerical study, a long existing confusion on hot wire near wall corrections was finally resolved (see also [37] and [38]).

Buoyancy driven flow in a Czochralski crucible

Czochralski (CZ) crystal growth is one of the most popular methods of producing large single crystals for electronic and photonic devices. Most industries producing silicon crystals, III-V crystals and crystals of oxide materials use the CZ process. Due to the importance for the single crystal production and its technological impact on the semi-conductor industry, there have been extensive research studies in the past couple of decades for thorough fundamental understanding of mechanisms governing the Czochralski process. The objective has been to improve as well as further optimize the process for larger crystals (*e. g.*, 0.3 - 0.4 m diameter) of high quality.

It has been pointed out by several researchers that the fluid flow in the Czochralski melt plays a major role on the crystal quality; the fluid flow in the CZ melt is the single most important phenomenon controlling transport of species such as oxygen and, in turn, purity of the crystal. The flow in the silicon melt is governed by several interacting forces such as buoyancy, Coriolis and centrifugal forces. The melt is maintained above the solidification point through controlled heating of the crucible which results in thermal buoyancy in the melt. In order to homogenize the thermal asymmetries resulting from external heating, the crucible is rotated. The uniformity at the crystal/melt interface is also improved by rotating the crystal while pulling to generate von Kàrmàn-Cochran centrifugal flow with its constant boundary layer thickness. The most important and interesting aspect of the flow in a CZ melt is the breakdown of the axisymmetric nature of the field leading to a host of interesting alternative flow patterns including non-periodic time dependent flows.

The fluid flow and heat transfer in an industrial Czochralski melt was analyzed by solving the time dependent three dimensional Navier-Stokes equations on curvilinear boundary fitted grids in a rotating frame of reference. The numerical methodology implemented in FASTEST-3D was extensively validated based on two different test cases [27, 29]. In order to represent the ellipsoidal crucible, a grid with about 1.73 million control volumes was generated in six blocks. Using the natural advantage of block structuring, computations were carried out on a parallel vector machine (NEC SX-4) with an optimal load balancing efficiency of 100% using four processors with a total performance of about 3.0 GFlops. The simulation shown here was performed for a laboratory scale crucible with a diameter D_c=0.339 m and height H_c=0.1 m, while the crystal has a diameter D_x=0.1 m. The crucible rotates with an angular velocity of Ω_c = 5 rpm, whereas the crystal rotates in the opposite direction with Ω_c = -20 rpm. A measured temperature distribution was prescribed at the crucible walls, while at the crystal/melt interface the solidification temperature was assumed. At the free surface of the melt, surface tension was not taken into account and heat loss took place by radiation. The most important non-dimensional parameters for this flow are the Rayleigh number Ra = $5.3 \cdot 10^6$, the Reynolds number Re = $7.9 \cdot 10^3$ and the Prandtl number Pr = 0.0106, which is very low for liquid silicon.

Simulations of the flow field were performed with and without a buoyancy extended k-ε turbulence model. It was found that this turbulence model suppresses the fluid mechanical instabilities caused by the interaction of buoyancy, centrifugal and Coriolis forces leading to an axisymmetric flow and thermal field, while the simulations without any turbulence model (semi-DNS: The synonym „semi-DNS" implies a fine computational grid, which, however, is insufficient for the resolution of all scales down to the Kolmogorov length) were found to predict the three dimensional and time dependent features of the melt flow well. As an example, Figs. 21 and 22 show the instantaneous flow structure and thermal field in a horizontal and a vertical cut through the centre of the crucible.

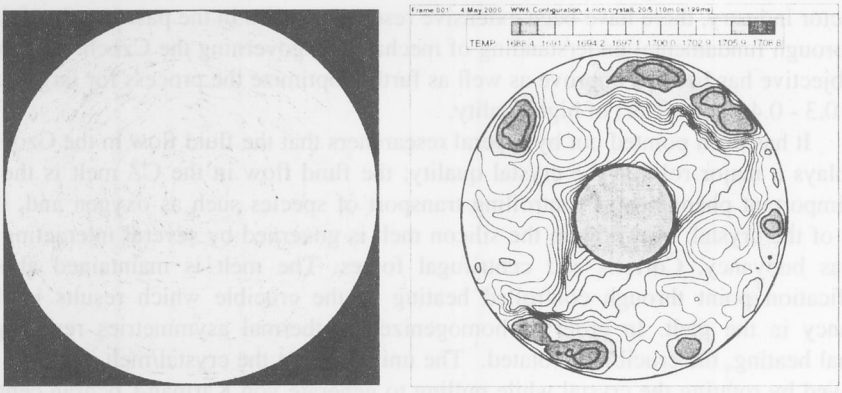

Figure 21. Three dimensional, time dependent turbulent flow visualized by LIC (left) and temperature distribution (right) in an industrial Czochralski crucible, horizontal plane directly below the free surface

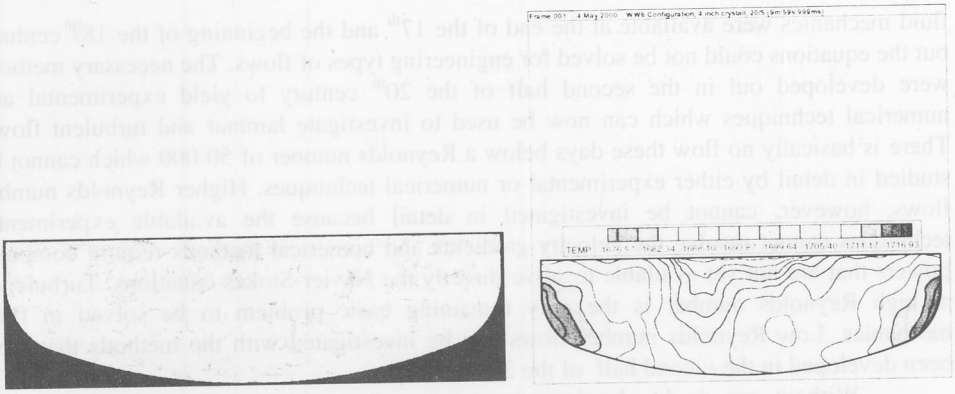

Figure 22. Three dimensional, time dependent turbulent flow visualized by LIC (left) and temperature distribution (right) in an industrial Czochralski crucible, vertical plane through the centre of the crucible

As expected from experimental observations, the predicted flow and temperature field is highly non-axisymmetric consisting of multiple vortices and buoyant plumes which rise from the bottom of the crucible up to the free surface visible in Fig. 21. Looking at animations of the simulations leads to the conclusion that these plumes rotate with an angular velocity similar to the crucible rotation rate Ω_c. Strong temperature fluctuations are also observed in the vicinity of the crystal which may influence the growth rate and finally the quality of the single crystal. Unfortunately, it is very difficult to measure the temperature distribution in the entire liquid melt. Therefore, comparisons between predictions and measurements are restricted to selected locations in the crucible. For that reason, the time history of the temperature at several positions in the melt was actually recorded in order to compare with measurements carried out by the Institute of Materials Science, University of Erlangen-Nürnberg. Based on mean values, standard deviations and spectra of the measured and predicted signals, a detailed validation of the computational approach can be performed. Preliminary results point out a reasonable agreement between measurements and predictions. Since the computations provide three dimensional, time resolved data of the entire melt flow, they are a very powerful tool for the analysis of the Czochralski system. In the future, the oxygen transport in the melt will be additionally taken into account in order to investigate this important phenomenon for the quality of the growing crystal (see also [27-30]. Additional applications and interesting results are presented in the paper by Breuer *et al.* in the present issue.

CONCLUSION

In this review we have shown that fluid mechanics research has a long history and was initially embedded in fields such as mathematics and physics. Hence, basic equations of

fluid mechanics were available at the end of the 17th and the beginning of the 18th century, but the equations could not be solved for engineering types of flows. The necessary methods were developed out in the second half of the 20th century to yield experimental and numerical techniques which can now be used to investigate laminar and turbulent flows. There is basically no flow these days below a Reynolds number of 50 000 which cannot be studied in detail by either experimental or numerical techniques. Higher Reynolds number flows, however, cannot be investigated in detail because the available experimental techniques cannot resolve the velocity gradients and numerical methods require computer powers that are not yet available to solve directly the Navier-Stokes equations. Turbulence at high Reynolds number is the only remaining basic problem to be solved in fluid mechanics. Low Reynolds number flows can be investigated with the methods that have been developed in the second half of the 20th century.

Without any doubt, developments of experimental and numerical methods will continue in the years ahead. There will be a change in fluid mechanics research, however, as can already be observed today, towards the application of methods to study fluid flows. The golden age of fluid mechanics has started. Fluid flows can be studied using well developed, currently available experimental and numerical techniques.

REFERENCES

[1] Van Dyke, M.: *An Album of Fluid Motion*, Parabolic Press, Stanford, California, (1982)

[2] Hama, R.F.: Streaklines in a perturbed shear flow, Physics of Fluids 5, (1962), pp. 644-650

[3] Eckelmann, H.: *Einführung in die Strömungsmesstechnik*, Teubner Studienbücher Mechanik, B.G. Teubner, Stuttgart, (1967)

[4] Bruun, H.H.: *Hot-Wire Anemometry: Principles and Signal Analysis*, Oxford University Press Inc. New York, (1995)

[5] Lumley, J.L.: *Stochastic Tools in Turbulence*, Academic Press, New York, (1970)

[6] Durst, F., Melling, A., Whitelaw, J.H.: *Principles and Practice of Laser-Doppler Anemometry*, Second Edition, Academic Press, New York, (1981)

[7] van de Hulst, H.C.: *Light Scattering by Small Particles*, Wiley Press, New York, (1957)

[8] Kerker, M.: *The Scattering of Light and oher Electromagnetic Radiation*, Academic Press, New York, (1969)

[9] Hjelmfelt, A.T., Mockros, L.F.: Motion of discrete particles in a turbulent fluid, Appl. Sci. Res. 16, (1966), p. 149

[10] Durst, F.: Scattering phenomena and their application in optical anemometry, Zeitschrift für Angewandte Mathematik und Physik 24, (1973), p. 619

[11] Durst, F., Zaré, M.: Laser-Doppler measurements in two-phase flows, Proceedings of the LDA-Symposium Copenhagen, (1975), pp. 403-429

[12] Hirleman, E.D.: History of development of the phase-doppler particle-sizing velocimeter, Part. Part. Syst. Charact. 13, (1996), pp. 59-67

[13] Naqwi, A., Durst, F., Liu, X.: Two optical methods for simultaneous measurement of particle size, velocity and refractive index, Applied Optics, 30, (1991), pp. 4949-4959

[14] Gouesbet, G.: Generalized Lorenz-Mie theory and applications, Part. Part. Syst. Charact. 11, (1994), pp. 22-34

[15] Uemura, T., Yoshimoto, M., Tatumil, M., Kaga, A.: Simultaneous multiple pixel processing algorithms for PTV and PIV, Developments in Laser Techniques and Fluid Mechanics, Selected Papers from the 8th Int. Symp. on Applications of Laser Anemometry to Fluid Mechanics, Ladoan, Portugal, (1997)

[16] Adrian, R.J.: Statistical properties of particle image velocimetry measurements in turbulent flow, Laser Anemometry in Fluid Mechanics – III, Selected Papers from the Third Int. Symp. on Applications of Laser Anemometry to Fluid Mechanics, Ladoan, Portugal, (1988)

[17] Meyers, J.F., Lee, J.W.: Three component Doppler global velocimeter measurements of the flow above a delta wing, Procedings of the 6th Int. Symp. Lisbon, Portugal, 20-23 July 1992, Springer-Verlag, Berlin, (1993), pp. 345-363

[18] Durst, F., Schäfer, M., Wechsler, K.: Efficient simulation of incompressible viscous flows on parallel computers, In: Flow Simulation with High-Performance Computers II, Notes on Numerical Fluid Mechanics, vol. 52, Vieweg, Braunschweig, (1996), pp. 87-101

[19] Durst, F., Schäfer, M: A parallel block-structured multigrid method for the prediction of incompressible flows, Int. J. Num. Methods Fluids, 22, (1996), pp. 549-565

[20] Khier, W., Breuer, M., Durst, F.: Flow structure around trains under side wind conditions: a numerical study, Int. J. Computers and Fluids, 29, (2000), pp. 179-195

[21] Khier, W., Breuer, M., Durst, F.: Numerical computation of 3-D turbulent flow around high speed trains under side wind conditions, TRANSAERO - a European initiative on transient aerodynamics for railway system optimisation, B. Schulte-Werning, R. Gregoire, A. Malfatti and G. Matschke (eds.), Proc. of the Brite/Euram Project Symp. 'Transient Aerodynamics for Railway System Optimisation', May 4--5, 1999, Paris, France, Notes on Numerical Fluid Mechanics, Springer Verlag, vol. 79, (2001).

[22] Wechsler, K., Breuer, M., Durst, F.: Steady and unsteady computations of turbulent flows induced by a 4/45° pitched blade impeller, J. Fluids Engineering, 121 (2), (1999), pp. 318-329

[23] Bartels, C., Breuer, M., Wechsler, K., Durst, F.: CFD-applications on parallel-vector computers: Computations of stirred vessel flows, Int. J. Computers and Fluids, 31, (2001), pp. 69-97

[24] Bartels, C., Breuer, M., Durst, F.: Comparison between direct numerical simulation and k-ε model prediction of the flow in a vessel stirred by a Rushton turbine, 10th European Conference on Mixing, Delft University of Technology, The Netherlands, July 2-5, (2000)

[25] Glück, M., Breuer, M., Durst, F., Halfmann, A., Rank, E.: Computation of fluid-structure interaction on lightweight structures, Fourth Int. Colloq. on Bluff Body Aerodynamics & Applications, Bochum, Germany, Sept. 11-14, 2000, Int. J. of Wind Engineering and Industrial Aerodynamics, 89, (2001), pp. 1351-1368

[26] Glück, M., Breuer, M., Durst, F., Halfmann, A., Rank, E.: Computation of wind-induced vibrations of flexible shells and membranous structures, subm. to J. Fluids and Structures, (2001)

[27] Basu, B., Enger, S., Breuer, M., Durst, F.: Three-dimensional simulation of flow and thermal field in a Czochralski melt using a block-structured finite-volume method, J. Crystal Growth, vol. 219/1-2, (2000), pp. 123-143

[28] Basu, B., Enger, S., Breuer, M., Durst, F.: Effect of crystal rotation on the three-dimensional mixed convection in the oxide melt for Czochralski growth, 3rd Int. Workshop on Modeling in Crystal Growth, Stony Brook, New York, USA, Oct. 18-20, (2000), J. Crystal Growth, 230/1-2, (2001), pp. 148-154

[29] Enger, S., Basu, B., Breuer, M., Durst, F.: Numerical study of three-dimensional mixed convection due to buoyancy and centrifugal force in an oxide melt for Czochralski growth, J. Crystal Growth, 219/1-2, (2000), pp. 144-164

[30] Enger, S., Gräbner, O., Müller, G., Breuer, M., Durst, F.: Comparison of measurements and numerical simulation of melt convection in Czochralski crystal growth of silicon, 3rd Int. Workshop on Modeling in Crystal Growth, Stony Brook, New York, USA, Oct. 18-20, 2000, J. Crystal Growth, 230/1-2, (2001), pp. 135-142

[31] Breuer, M.: Large eddy simulation of the sub-critical flow past a circular cylinder: numerical and modeling aspects, Int. J. Num. Methods Fluids, 28, (1998), pp. 1281-1302

[32] Breuer, M.: A challenging test case for large eddy simulation: high Reynolds number circular cylinder flow, Int. J. Heat Fluid Flow, 21, (2000), pp. 648-654

[33] Breuer, M., Bernsdorf, J., Zeiser, T., Durst, F.: Accurate computations of the laminar flow past a square cylinder based on two different methods: Lattice-Boltzmann and Finite-Volume, Int. J. Heat Fluid Flow, 21, (2000), pp. 186-196

[34] Breuer, M.: Direct Numerical Simulation and Large-Eddy Simulation of Turbulent Flows with High-Performance Computers (in German), Habilitation Thesis, University of Erlangen--Nürnberg, Germany, (2001).

[35] Breuer, M., Jovicic, N.: Separated flow around a flat plate at high incidence: an LES investigation, Second Int. Symposium on Turbulence and Shear Flow Phenomena, Stockholm, Sweden, June 27-29, 2001, vol. III, pp. 393-398, J. of Turbulence, in press, (2001).

[36] Breuer, M., Jovicic, N.: An LES Investigation of the separated flow past an airfoil at high angle of attack, Proc. of the 4th Workshop on Direct and Large Eddy Simulation, Enschede, The Netherlands, July 18-20, 2001, ERCOFTAC Series, vol. 8, Direct and Large-Eddy Simulation IV, eds. B.J. Geurts, R. Friedrich, O. Mètais, Kluwer Academic Publishers, Dordrecht, (2001).

[37] Durst, F., Shi, J.M., Breuer, M.: Numerical prediction of hot-wire corrections near walls, J. Fluids Engineering, in press, (2001).

[38] Shi, J.M., Breuer, M., Durst, F.: Wall effect on heat transfer from a micro cylinder in near-wall shear flow, Int. J. Heat and Mass Transfer, 45/6, (2002), pp. 1309-1320

Authors' addresses:

S. Oka
Institute of Nuclear Sciences
Vinča
P.O. Box 522
11001 Belgrade
Yugoslavia

D. Melling
Institute of Fluid Mechanics
University of Erlangen-Nürnberg
Cauerstr. 4, D-91058 Erlangen
Germany

Paper submitted: November 30, 2001
Paper revised: February 26, 2002
Paper accepted: March 18, 2002